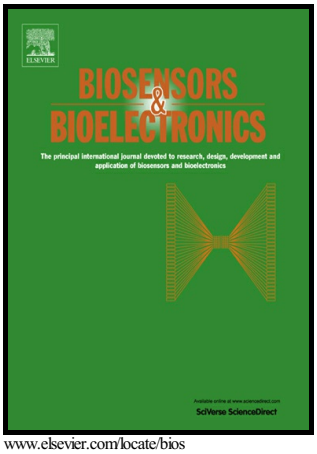

www.elsevier.com/locate/bios

Broccoli-shaped Biosensor Hierarchy for Electrochemical Screening of Noradrenaline in Living Cells

M.Y. Emran, M. Mekawy, N. Akhtar, M.A. Shenashen, I.M. EL-Sewify, A. Faheem, S.A. El-Safty

PII: S0956-5663(17)30585-7
DOI: http://dx.doi.org/10.1016/j.bios.2017.08.050
Reference: BIOS9960

To appear in: *Biosensors and Bioelectronic*

Received date: 4 June 2017
Revised date: 21 August 2017
Accepted date: 22 August 2017

Cite this article as: M.Y. Emran, M. Mekawy, N. Akhtar, M.A. Shenashen, I.M. EL-Sewify, A. Faheem and S.A. El-Safty, Broccoli-shaped Biosensor Hierarchy for Electrochemical Screening of Noradrenaline in Living Cells, *Biosensors and Bioelectronic,* http://dx.doi.org/10.1016/j.bios.2017.08.050

Broccoli-shaped Biosensor Hierarchy for Electrochemical Screening of Noradrenaline in Living Cells

M.Y. Emran[1], M. Mekawy[1], N. Akhtar[1], M.A. Shenashen[1], I. M. EL-Sewify[1], A. Faheem[2], S. A. El-Safty[1,*]

[1] National Institute for Materials Science (NIMS), Research Center for Functional Materials, 1-2-1 Sengen, Tsukuba-shi, Ibaraki-ken, 305-0047, Japan.
[2] School of Pharmacy and Pharmaceutical Sciences, Faculty of Health Sciences and Wellbeing, University of Sunderland, Sunderland, SR1 3SD, UK.

Abstract

Monitoring and determination of ultra-trace concentrations of monoamine neurotransmitter such as noradrenaline (NA) in living cells with simple, sensitive and selective assays are significantly interesting. We design NA-electrode sensing system based on C-, N-doped NiO broccoli-like hierarchy (CNNB). The spherical broccoli-head umbrella architectures associated with nano-tubular arrangements enabled to tailor NA biosensor design. The homogenous doping and anisotropic dispersion of CN nanospheres along the entire NB head nanotubes lead to creating of abundant electroactive sites in the interior tubular vessels and outer surfaces for ultrasensitive detection of NA in living cells such as PC12. The CNNB biosensor electrodes showed efficient electrocatalytic activity, enhanced kinetics for electrooxidation of NA, and fast electron-transfer between electrode–electrolyte interface surfaces, enabling synergistic enhancement in sensitivity, and selectivity at a low-detectable concentration of ~ 6 nM and reproducibility of broccoli-shaped NA-electrodes. The integrated CNNB biosensor electrodes showed evidence of monitoring and screening of NA released from PC12 cells under K^+ ion-extracellular stimulation process. The unique features of CNNB in terms of NA-selectivity among multi-competitive components, long-term stability during the detection of NA may open their practical, in-vitro application for extracellular monoamine neurotransmitters detection in living cells.

Keywords: Noradrenaline; Biosensors; Broccoli-shaped hierarchy; Electrochemical screening; living cells.

1. Introduction

Catecholamine neurotransmitters (CAs) such as adrenaline (A), noradrenaline (NA) and dopamine (DA) are biogenic amines. These neurotransmitters play an important role in neurotransmission and other physiological processes. It is well-known that the high concentration level of CAs may lead to a significant effect on the cardiovascular system and myocardial infarction. In turn, the low concentration level of CAs may cause a low blood pressure (Bergquist and Silberring 1998; Braestrup et al. 1974; Knigge et al. 1999; Nikolelis et al. 2003; Nikolelis et al. 2005). Among all CAs, noradrenaline is a hormone secreted mainly from the adrenal medulla. NA is regarded as a metabotropic neurotransmitter in the sympathetic nervous system from nerve endings and some areas of the cerebral cortex (Andén et al. 1965; Glowinski et al. 1965).

Variable analytical techniques including fluorescence microscopy (Wachman et al. 2004), high-performance liquid chromatography (Zhang et al. 2003), capillary electrophoresis (Lapainis et al. 2007), and spectrophotometry (Nasirizadeh and Zare 2009) were used to controlled monitoring the CAs (such as NA) from both dopaminergic cell populations and striatal brain slices. However, most of these techniques are expensive; they also require sophisticated instruments to maintain and run, and the procedures for preparation of biosensors are rather time-consuming.

The PC12 cell lines were used for neurotransmitters source because they enabled to maintain the same original characteristics of mature sympathetic neurons (Lapainis et al. 2007). Electrochemical methods have been suitable and often employed in the clinical analysis to determine the concentration of CAs. These methods featured easy operation, cost-effectiveness, and sensitivity to real-time monitoring of the CA targets (Devnani et al. 2016). Simultaneously selective determination of noradrenaline in the coexisting of molecules like ascorbic acid, acetaminophen, tryptophan, xanthine, and caffeine using modified glassy carbon or carbon paste electrodes were reported (Akhgar et al. 2012; Beitollahi and Mohammadi 2013; Chandra et al. 2013; Knez et al. 2006; Taei and Jamshidi 2017).

Nanomaterials based metal-oxide semiconductors are promising in the biosensing functionality because of their good biological compatibility, large surface area, and special physical and chemical properties (Shenashen et al. 2017a; Shenashen et al. 2016; Shenashen et al. 2017b). NiO semiconductors has intrinsic properties, including supreme chemical stability, facile charge transfer along active surfaces, efficient electrocatalysis, low cytotoxicity, and high biological compatibility (Dong et al. 2011; El-Safty et al. 2008; Khairy and El-Safty 2013, 2014,

2015; Liu et al. 2013; Salimi et al. 2007; Xiang et al. 2002; Yang et al. 2011). These features enabled NiO to effectively construct electrochemical biosensor. Fabrication of carbon materials in wide range morphologies such as dots, sheets, nanotubes, nanospheres enhanced the electrode surface activities (Akhtar et al. 2016; Akhtar et al. 2015b; Ali et al. 2017; El-Safty et al. 2017; Hassen et al. 2016a; Hassen et al. 2016b; Shenashen

et al. 2017b). Anisotropic doing of active sites leads to facilitate the mass transport at the electrode-electrolyte interface (Ma et al. 2014). For instance, metal- or metal oxide-doped carbon such as NiO@carbon–nitrogen dot electrodes (Zhang et al. 2015), NiAl-LDH carbon dots (Sun et al. 2011), NiCo N-doped carbon nanoplates (Zhang et al. 2015), CuO@3D graphene (Ma et al. 2014), Au@carbon dots chitosan composite film (Huang et al. 2014), AuNPs immobilized on pre-treated graphene/CNT (Abdelwahab 2016), and Pt@graphene nanocomposites (Sun et al. 2011) can be used a wide-range of biosensing applications.

In this paper, the design of modified electrode with high electrocatalytic activity and monitoring of NA secreted of from living cells was fabricated based on C-, N-doped NiO broccoli-like hierarchy (CNNB). The unique geometrical and morphological structures are the key roles for the electrocatalytic performance. The CNNB exhibits unique morphologies of a broccoli-like hierarchy with single-head (NB-1) structure, and two asymmetric heads spread out in opposite direction and connected with a trunk (NB-2). The vertical alignment of the tubular pipes throughout the entire broccoli head structure is the key role for the fast electron transfer and the electrocatalytic activity of NB modified electrodes. The CN nanospheres doped NB with homogeneity at outer and entire head nanotubes, lead to facilitate the interaction between the biomolecules and the active catalytic surface sites. The CNNB shows analytical integration process for detection of mono-biomolecules such as AA, DA, A, UA and NA with high-impact on monitoring of NA. The integrated CNNB biosensor electrodes showed monitoring of NA released from PC12 cells under K^+ stimulation process. The CNNB can be employed for the application of in vitro detection of NA released from living cells with low cytotoxicity and high biocompatibility.

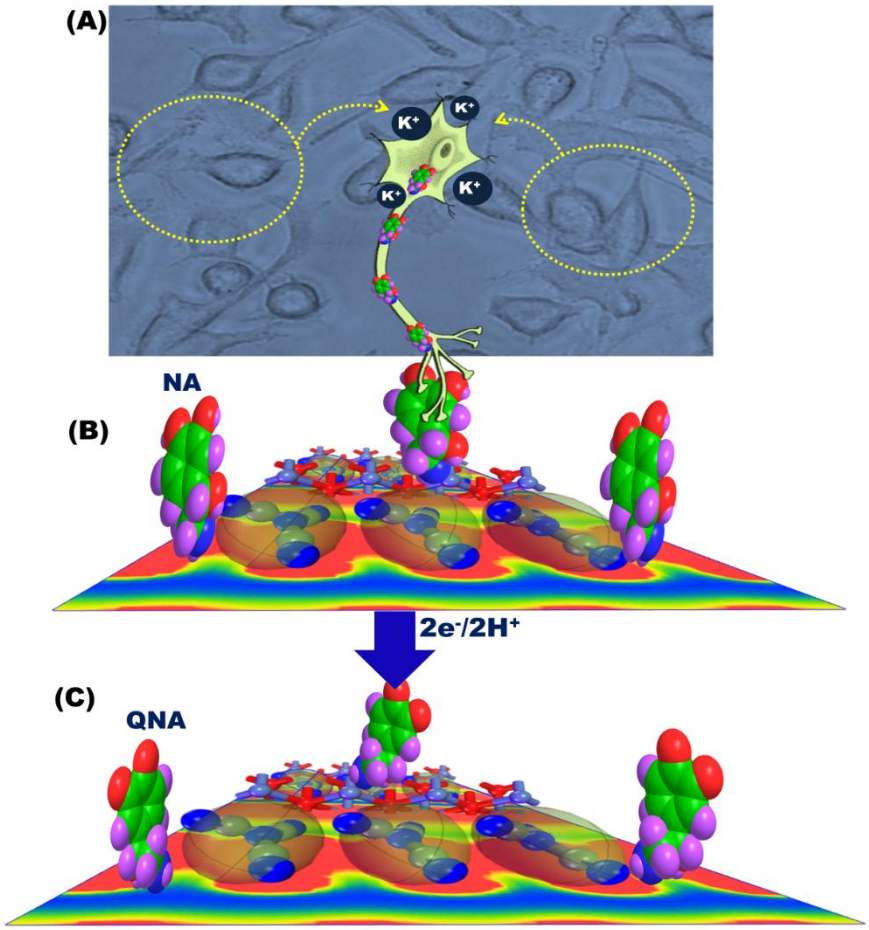

Scheme 1. A) Confocal microscopy of PC12 incubated with 30 mM KCl providing the section of extracellular noradrenaline. B) Binding of noradrenaline at the surface of CNNB-1 with corresponding {110} crystal plane. C) The oxidized form of noradrenaline; which converted to quinone form with losing of $2e^-/2H^+$.

2. Materials and methods

2.1. Synthesis of CNNB-1 and CNNB-2

Nickel oxide broccoli like with a single head (NB-1) and with the asymmetric double head (NB-1) were fabricated via one-pot hydrothermal synthetic approach. The synthesized NB were prepared according to the following procedure: 1 mM of $Ni(NO_3)_2 \cdot 6H_2O$ was dissolved in a 100-mL volumetric flask containing 15 mL deionized water and stirred until dissolved at room temperature. Then, 15 mL of 1 mM solution of ammonium hydrogen phosphate ($(NH_4)_2HPO_4$) in deionized water was added to the stirred solution of $Ni(NO_3)_2 \cdot 6H_2O$ with a definite flow rate to control the shape (see supporting information, Scheme S1). The prepared solution was transferred into a 100-mL Teflon-lined stainless-steel autoclave, sealed and maintained at

160 °C for 8h. After the required time, a green precipitate appeared because of NiO formation. The precipitate was then rinsed with ultrapure water/absolute ethanol to remove the soluble impurities. The NiOOH samples with different hierarchal structures were dried in an oven at 80 °C and annealed at 400 °C for 4h to obtain NiO broccoli like structures with a single head (NB-1) and asymmetric double heads (NB-2).

Carbon-nitrogen nanospheres doped NB-1 and NB-2 were constructed as follows: 60 mg of prepared NB was dispersed in 100 mL of tris-buffer solution (pH 8.5), ultrasonication for 2h followed by the addition of purified aniline (20 mM). Then, 20 mM of potassium persulfate in 0.1 M HCl solution was added dropwise to the stirred solution at 0 °C. The composite materials were stored for 12h at room temperature, and the obtained aniline-polymerized NB samples were washed several times with deionized water. The same procedure was repeated three times. Finally, the polyaniline-coated NB was calcined at 500 °C for 4h in an argon atmosphere to obtain C-N nanospheres doped NB.

2.2. Cell culture

PC12 cell line was obtained from PC12 (ATCC® CRL1721™) and was cultured by incubation under 5% CO_2 at 37 °C in Dulbecco's Modified Eagle's Medium containing 5% fetal bovine serum, 10% heat-inactivated serum. The culture medium was replaced every 3 to 4 days.

3. Results and discussion

The morphological growth of NB is combined with the building of nanostructures using structure-directing agent templates ($(NH_4)_2HPO_4$) under hydrothermal treatment conditions (see scheme S1). Generally, the initial precursor ($Ni(NO_3)_2{\cdot}6H_2O$, $(NH_4)_2HPO_4$) and the as-obtained broccoli-like construction NB with single (1) or asymmetric double head (2), can be produced from successive reactions. Briefly, the $(NH_4)_2HPO_4$ hydrolysis generates active OH^- and PO_4^{3-} anions during HT process. These anions subsequently reacted with Ni^{2+} ions to form (i) NiOOH frameworks, (ii) broccoli-shaped hierarchy, and (iii) formation of tubular-like needles-decorated the broccoli structures. The time-dependent, dropwise addition of PO_4^{3-} anions with a definite flow rate not only controlled the formation of hierarchical NiO broccoli structures but also the morphological shapes of the broccoli heads, as shown in scheme S1. The PO_4^{3-} anions possess massive negative charges which may act as a mediator for the creation of tubular branches that spread out along the broccoli head formation. The electrostatic binding between positive-charged Ni^{2+} ions and negative-charged PO_4^{3-} ions was a driving force to create broccoli-shaped structures with head and trunk (see Figure 1& Scheme S1). As a result, the time-dependent

addition of PO_4^{3-} anions plays key roles in the formation of broccoli-shaped NiO architecture with a single or an asymmetric double head that connected by a trunk or a dipole rod. Head construction may also be attributed to the stereo PO_4^{3-} shape in its solution, which directly stimulates the binding with Ni^{2+} and then the crystal growth depth along the entire structures.

Carbon-nitrogen nanospheres were doped along with the hierarchal NiO structures without distortion. During the doping process, a thin film of polyaniline was polymerized at 0 °C after dropwise addition of potassium persulfate with continuous stirring. Potassium persulfate generates the free radical monomer, forming a homogenous black precipitate of polyaniline at NB surface. Carbonization process of polyaniline at 500 °C, in Ar gas flow, leads homogenous dispersion of C-N nanospheres-doped NiO.

3.1 Structure features of CNNB-1 and CNNB-2

Well-controlled morphology and high stable construction of NB formation were provided using field-emission scanning electron microscopy (FE-SEM) and transmission electron microscopy (TEM) images. Figure 1 shows the FE-SEM and scanning transmission electron microscopy (STEM) of the prepared materials at different flow rates as in scheme S1, and the formation of CN-nanospheres at its surface leads to the creation of CNNB with asymmetric double heads (CNNB-2) and symmetric head (CNNB-1) broccoli like morphology. Figure 1A illustrates the construction of NB-1 unit, which is like a broccoli with head and trunk. Focusing on different points of view demonstrate the homogeneity and unity of the new structure of NB with a stable formation, as in the vertical back of view for NB-1 (B) and CNNB-1(C). High-magnification FE-SEM images (B) represent the following dimensions of the NB-1; average head diameters ranging from 3 µm to 4 µm and trunk diameter from 1 µm to 1.5 µm. Figure 1C shows the homogeneity of CN-nanospheres at the NB-1. The head construction shows an exceptional construction obtained from TEM images in Fig. 1D, where the head surface is like a hedgehog's skin, consisting of thick nanotubes spread from the inner trunk to the outer surface with formation of tunable vessels. The formation of NB with two heads spread out on opposite sides and connected by a trunk in between is shown in scheme S1 (Figs. 1E–1G). Figures 1E and 1F show the FE-SEM of another construction of NB, which is a broccoli-shaped morphology with two heads and one trunk. Vertical alignment for one unit of NB-2 showed the structure stability and head morphology.

Further confirmation of stable NB-2-unit construction is shown in Fig. 1F. The NB-2 construction consists of two heads and a trunk with distinct size; the bigger head size is approximately 5 to 6 µm, while the smaller one is ranged from 2 to 2.5 µm, and the trunk size is

ranged from 1 to 1.5 μm. The FE-SEM image of CNNB broccoli-like hierarchy shows evidence of the formation of a unique morphology. The microscopic images show the formation of well-aligned nanotubes at the surface ends of the whole head that was like a jagged surface. High magnification using high-angle annular dark-field (HAADF)-STEM focusing on the tubes at the head surface ends shows the complete morphological constructions (Figs. 1H and 1I). The head nanotubes shape is confirmed by HAADF-STEM and the tube size is approximately 20 nm, with CN homogenous covering the surface of NB. Electron diffraction (ED) focusing on nanotubes surfaces reflects the degree of the crystalline structure of NB, as shown in Figs. 1J and its inset, 1K, and 1L. The broccoli-shaped heads featured needle-top surfaces with highly atomic arrangements along predominant the {110} crystal plane in all directions, orientations (Fig. 1K) and edges (inset of Fig. 1J). Confirmation from ED resolution of low- and high-index lattice planes of (−1–11), (002), (1–11), (−220), (−11–1), (00–2), (1–1–1), and (2–20) fringes around the bottom {110}–principle zone–dominant plane was shown in the inset of Fig. 1H. Thus, the designed materials possess i) a smooth surface, which has a significant effect on the contact surface between the electrolyte and the designed electrode surface with enhancing the fast response of targets, ii) numerous number of active sites with exposure of the NB unit for the opposite electrolyte, because of the unique morphology (head with a trunk or two heads with a trunk). The intrinsic catalytic activity was increased, related to the unique construction of each unit of NB which was directly decoded as active sites.

Sharp and well-resolved diffraction peaks for the NB are found in the wide-angle X-ray diffraction (WA-XRD) patterns as shown in Fig. 1N (green line), which is consistent with JCPDS no. 01-089-5881 (i.e., a face-centered cubic Fm3m symmetry with the lattice constant (α = 8.35 Å) (Akhtar et al. 2016; Khairy and El-Safty 2013, 2014, 2015; Khairy et al. 2012). However, WA-XRD profile of CN-nanospheres doped NB-1 and NB-2 (Fig. 1N (red line)) are found to keep the characteristic diffraction peaks of face-cantered cubic NiO (JCPDS no. 01-089-5881), along with a broad peak at 2θ = 24.61, indicating the existence of carbon (Dong et al. 2011; Hassen et al. 2016b; Shenashen et al. 2016; Shenashen et al. 2017b).

To confirm the existence of carbon, material structure, and samples functional groups; Raman shift spectrum was used at the excitation wavelength of 532 nm (Fig. S2A). The peaks at 532 cm^{-1}, 760 cm^{-1}, and 1085 cm^{-1} are attributed to one phonon (1P)(TO), (2P) (2TO) modes, and 2LO (longitudinal optical) modes, respectively, indicating the presence of pristine NiO for NB samples (Akhtar et al , 2016; Akhtar et al , 2015). The CNNB provides two distinct peaks in CNNB-1and CNNB-2 corresponds to D (~1366 cm^{-1}) and G (~1500 cm^{-1}) bands originating from the disordered carbon and sp^2 clusters, respectively (Hassan et al. 2016; Hassen et al.

2016b; Shenashen et al. 2017a; Shenashen et al. 2016) (for more details see supporting information).

The N_2 adsorption-desorption isotherm of NB samples featured type IV with H2-type hysteresis loop as in Fig. S2B. Figure 1M and the table inset show the NLDF pore distribution of NB-1, NB-2, CNNB-1 and CNNB-2, these data confirmed that NB-2, NB-1, and CNNB-2 has two types of pores (meso- and macropore) and provides the hierarchical structure of the prepared samples, while mesoporous structure is dominant for CNNB-1 with high surface area, as shown in Fig. 1M and its table inset (for more details see supporting information with Fig. S2(B&C) (El-Safty 2008; El-Safty et al. 2015a; El-Safty et al. 2015b; El-Safty and Shenashen 2013; El-Safty et al. 2012). Elucidations of surface components of CNNB, as well as NB, were performed by XPS measurements, where high-resolution XPS spectra of the Ni 2p, O 1s, C 1s, and N 1s peaks were performed for providing the chemical formations (for more details see supporting information and Fig. S3).

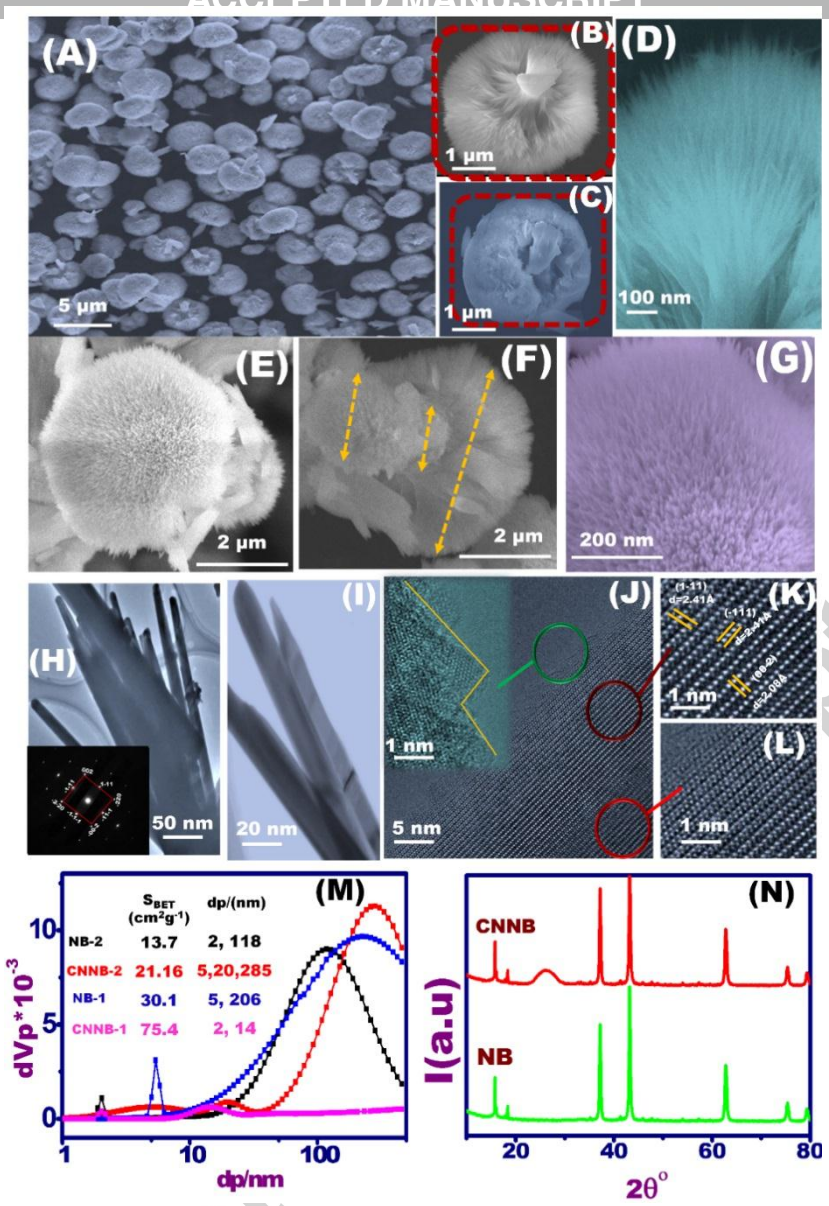

Figure 1. (A) FE-SEM micrograph for CNNB-1. (B) High magnification of FE-SEM for the unit construction of NB-1 from the vertical back of view. (C) High magnification of FE-SEM for NB-1 covered by CN-nanospheres from the vertical point of view. (D) HAADF-STEM micrograph focused on the head unit of NB-2 (E&F). (G) High magnification of FE-SEM focused on the head unit of CNNB-2. (H&I) High magnification of HAADF-STEM focusing on the tubes of the top head surface, inset high-dense ED-STEM with {110} crystal plane. (J) High magnification of HAADF-STEM focusing on the ends of tubes, focusing on the different degree of the tube at its center (K), denser for interior head (L) and at its top edge (inset of J). (M) NLDF pore size distribution. (N) XRD patterns of NB and CNNB. The table (inset of M) shows the pore size and S_{BET} for NB-2, NB-1, CNNB-2, and CNNB-1.

3.2. Surface configurations of microscopic CNNB-1and CNNB-2

The {110} and {101} close-packed plane and its surface atomic configurations, electron density difference maps, and pulse surface electrons in continuous generation modes around the NB-1 and NB-2 active sites are illustrated in Fig. 2A. The surface structure has a mesoporous framework around {110} planes, which increases the actively energetic surface coverage for easy diffusion which leads to high electron transport is shown in the electrolyte surface interfaces. Figure 2B illustrates the continuous electron streams on the top-level of {110} - orientation distributed closely to a central and focal point surface around the Ni^{2+} and O^{2-} vacancy sites of NB-1, and representing a localized network of the confinement electrostatic potential elevated to antedate the surface charge density around O and Ni atoms and effective potential molecules to Ni^{2+} site binding. In addition, Figures 2 (A-F) provide the {110}-surface active sites, containing the atomic O and Ni arrangements, CN surface electron clouds, and the {110}-surface electron density of CNNB-1, which are the key elements to activate the surfaces during the electro-oxidation reaction of noradrenaline, leading to enhance the sensitivity of CNNB electrode (Zhang et al. 2015).

The CNNB-1 geometric molecule-to-surface orientation generated numerous accessible surface sites and flexible interactions and thermodynamically stable bindings. Figures 2E and 2F show that the {110} and {101}-top-surface around double-layer surfaces provide high energy electron surfaces formed along the entire NB crystal structure directed along {110} and {101} surface exposure, particularly at the 4-Ni^{2+}-top surfaces (E) which enhances the electrocatalytic activity of Ni^{+2} with the target molecules. The surface configurations of CNNB-1 hierarchy oriented with exposed high-index facets along {110}- domains can feasibly create dense Ni^{2+} atoms and more electron-rich O^{2-} vacancy sites with delocalization charges of CN clouds, producing more efficient electron transport and NA-to-surface binding along the {110} exposed plane.

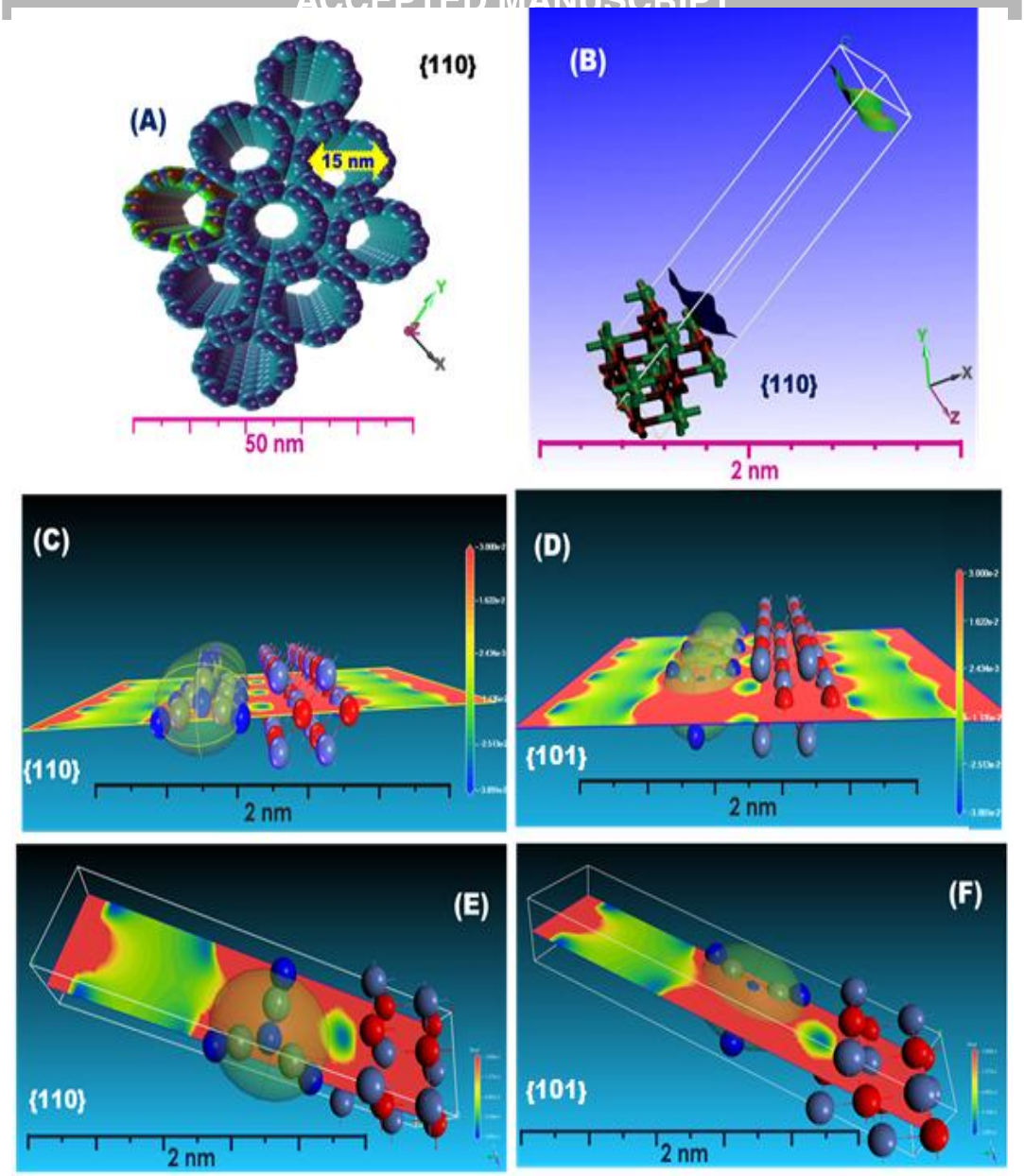

Figure 2. (A) Mesostructured {110}-NB crystal facet oriented around the mesopore frameworks. The location of the frame structure along {110} plane enabled the actively energetic surface coverage for facile diffusion and strong binding with the target molecules. (B) The atomic organization of NB-1 crystal into the exposed {110}-plane surface. (C, D) High energy surfaces formed along the entire crystal structure directed along {110} and {101} surface exposure and CN-nanospheres clouds over Ni and O atoms for NB-1 and NB-2, respectively. (E & F) {110} and {101}-top-surface around double-layer surfaces show high energy electron surfaces formed along the entire NB crystal structure directed along {110} and {101} surface exposure, particularly at the Ni^{2+}-top surfaces with CN clouds.

3.3. Electrocatalytic activity of the CNNB biosensor electrodes

The electrochemical behaviors of ITO, CNNB-2/ITO, and CNNB-1/ITO electrodes were investigated for providing the electrocatalytic activity, facile electron transfer, and molecular diffusion. Cyclic voltammetry (CV) technique was performed in 0.1 M PBS (pH 7.0) containing 1 mM hexacyanoferrate (III) $[Fe(CN)_6]^{3-}$ within the potential range of 0.0 V to 0.6 V (vs. Ag/AgCl) at scan rate of 100 mV/s (Fig. S4A). The $Fe(CN)_6]^{3-}$ was used as a redox probe to investigate key factors affected the selected electrodes, including electronic properties, surface structure, and surface chemistry (Akhtar et al. 2015a; Hassan et al. 2016). Figure S4A shows that the redox potential peak separation (ΔEp) value of CNNB-1/ITO (red line) (69 mV) was lower than that of the ITO (dark green line) (100 mV) and CNNB-2/ITO (wine line) (80 mV) electrodes. Furthermore, the anodic current of CNNB-1/ITO was higher than that of ITO and CNNB-2/ITO. This finding indicates the enhanced ion transmission performance at the electrode–electrolyte interface, and highly electrocatalytic activity of CNNB-1, thereby engaging greater fractions of catalytic active sites on the surface of the electrode for the Faradaic redox reaction.

The electron transfer and diffusion properties of ITO, CNNB-1/ITO, and CNNB-2/TIO were investigated using impedance spectroscopy measurements (EIS) (Fig. S4B). In an EIS measurement, there are two distinct parameters, the semicircle and the line, which related to the electron transfer resistance (Ret) of the electrode, and diffusion of the electroactive species, respectively (Akhtar et al. 2015a; Chen et al. 2014; Hassan et al. 2016; Hassen et al. 2016b). Typical Nyquist impedance plots of ITO, CNNB-2/ITO and CNNB-1/ITO electrodes in 0.1 M PBS (pH 7.0) are shown in Fig. S4B. The semicircle of the CNNB-1/ITO electrode shows further decrease than ITO and CNNB-2/ITO electrodes with extremely low Ret value and high conductivity. Thus, the CNNB-1/ITO electrode shows high catalytic activity due to the low resistance, large surface area, and high ion diffusion compared with ITO electrode and CNNB-2 biosensor. Furthermore, the surface charge and electron mobility and configuration along of the predominant {110}-NiO active sites of CNNB-1 are the main key values that boosted the electrode sensitivity.

3.4. Electrochemical behavior of CNNB-2 and CNNB-1 for mono-biomolecules

The electrochemical behaviors of mono-biomolecules such as NA, AA, A, DA, and UA on the CNNB-2 and CNNB-1 were measured using differential pulse voltammetry (DPV) in 0.1 M PBS (pH 7) at pulse height of 60 mV and pulse width 25 ms. Figure 3A shows the catalytic oxidation of 5 µM NA on CNNB-2 and CNNB-1. A significant DPV peak observed at applied

potential 0.17 V for CNNB-2 and CNNB-1, which corresponds to the oxidation of NA to o-quinone forms and provides that CNNB-1 has more sensitivity than CNNB-2. The same behavior is observed for 0.5 mM AA, 10 µM DA, 10 µM A, and 0.2 mM UA. The catalytic oxidation current of CNNB-1 is higher than that of CNNB-2 at onset potentials of 0.05, 0.31, 0.12 and 0.47 in 0.1 M PBS (pH 7) for AA, DA, A, and UA, respectively as shown in Figs. 3(B–E). The CNNB biosensor electrodes show high selectivity along with visualizing the peak separation (ΔE) between the coexisting molecules compared with NA were $\Delta E_{AA\text{-}NA}$ = 120 mV, $\Delta E_{A\text{-}NA}$ = 50 mV, $\Delta E_{DA\text{-}NA}$ = 140 mV, and $\Delta E_{AA\text{-}NA}$ = 300 mV. These findings show that the CNNB-1 biosensor electrode is sensitive for AA, A, DA, UA, and NA as a result of the enhancement in the electrocatalytic properties. The facile diffusion of biomolecules along the {110}-surface active coverage in the axially oriented direction of nano-tubular electrode design may lead to fast response and high sensitivity of CNNB-1 biosensor.

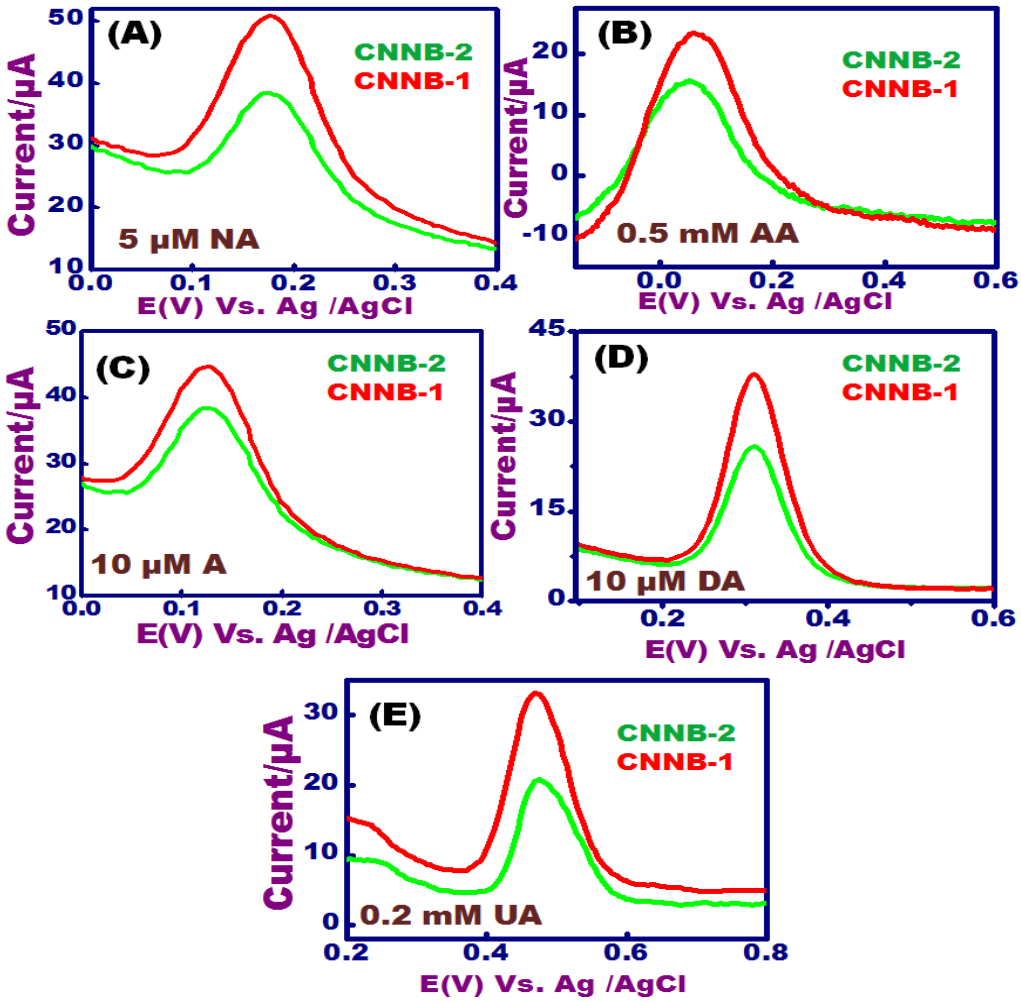

Figure 3. DPV of CNNB-2 (green line) and CNNB-1(red line) for 5 µM NA (A), 0.5 mM AA (B), 10 µM A (C) 10 µM DA (D) and 0.2 mM UA (E) in 0.1 M PBS (pH= 7) at scan rate = 100 mVs^{-1}, pulse height = 60 mV, pulse width = 25 ms.

3.5. Electrochemical detection of mono-biomolecules on CNNB-1 biosensor

The individual detection of mono-biomolecules such as NA, AA, A, DA, and UA on CNNB-1 biosensor electrode was examined by DPV in 0.1 M PBS (pH 7) at a pulse height of 60 mV and a pulse width of 25 ms. Figure S6A shows the current response of UA was increased with increasing UA concentrations from 25 µM to 600 µM; the linear regression equation was {I(µA) = 0.73 [UA](µM) + 26.62; R^2 = 0.99} (inset of Fig. S6A); therefore, the detection limit was calculated to be 15 µM based on the regression equation (S/N = 3). For AA, the current response was increased with increasing the AA concentrations from 50 µM to 2 mM; the linear regression equation was {I (µA) = 0.021 [AA](µM) + 19.7; R^2 = 0.99} and the detection limit was calculated to be 36 µM as presented in Fig. S6B and its inset. Furthermore, significant increasing of the oxidation peak upon increasing the concentrations of DA, A, and NA were observed on DPV signal of CNNB-1 biosensor in a range from 1 µM to 20 µM, indicating that the CNNB-1 biosensor electrode can be used for the sensitive detection of dopamine, adrenaline, and noradrenaline (Figs. S6C-E). By plotting the concentration versus the current for DA, A, and NA, the linear regression equations are I(µA)= 2.05 [DA](µM) + 0.64 (R^2 = 0.988), I(µA)= 1.46 [A](µM) + 22.31 (R^2 = 0.979) and I(µA)= 29.2 [NA](µM) + 44.79 (R^2 = 0.977) (inset of Figs. S6C-E). The detection limits were calculated to be 2.6, 2.86, and 0.35 µM for DA, A, and NA, respectively. Selectivity of CNNB-1 biosensor electrode for NA was clearly obtained from the detection limit of each target and illustrated in Fig. S6F, where the peak current response was high for NA compared with the other targets at the same concentration. Furthermore, no current response was found for AA and UA at the obvious concentrations of NA. These results illustrated the selectivity of CNNB-1 for biosensing of NA molecule.

3.6. wide-range sensitivity and long-term stability of CNNB-1 biosensor electrodes

NA-sensitivity on CNNB-1 at low concentrations is performed using the chronoamperometric technique at applied potential 0.17 V in 0.1 M PBS (pH 7) under stirring conditions. The amperometric response of NA was increased as step adding of 0.5 µM NA (Fig. 4A). The appearance of strong oxidation peak in fast response time within 10 s indicates the NA sensitivity using CNNB-1 biosensor electrode. The calibration curve shows a linear relationship with regression equation, I (µA) = 22.67 [NA](µM) + 4.32 (R^2 = 0.9997), as illustrated from Fig. 4B. The relative standard deviation (RSD) was estimated to be 2.5%, leading to the low detection limit of 6 nM. The CNNB-1 biosensor electrode exhibits high sensitivity for NA compared with other electrodes, as shown in Table S1. The CNNB-1 provides supreme

sensitivity compared with other NA modified electrodes. This finding indicates that the CNNB-1 biosensor electrode represents NA biosensor with high sensitivity and selectivity.

The reproducibility of the CNNB-1 biosensor electrode was evaluated. In such experimental protocols, the current responses are examined for multiple (≥5) CNNB-1 biosensor electrode in 10 µM NA concentration at the optimum sensing conditions of 0.1 M PBS (pH 7) and applied the potential of 0.17 V (vs. Ag/AgCl) at room temperature. The RSD of the five amperometric response assays ranged from 2.25%, as evidenced by the fitting plot of the response current graphs (Fig. S7(red column)). To confirm the reusability of a CNNB-1 biosensor electrode, the current responses as a function of five different samples with a constant concentration of NA (10 µM) were measured repeatedly after every washing of CNNB-1 biosensor electrode with distilled H_2O for three times at the optimum sensing conditions (Fig. S7(green column)). Thus, the reused CNNB-1 biosensor electrode showed high sensing response efficiency (i.e., 98%) despite five reuses/cycles.

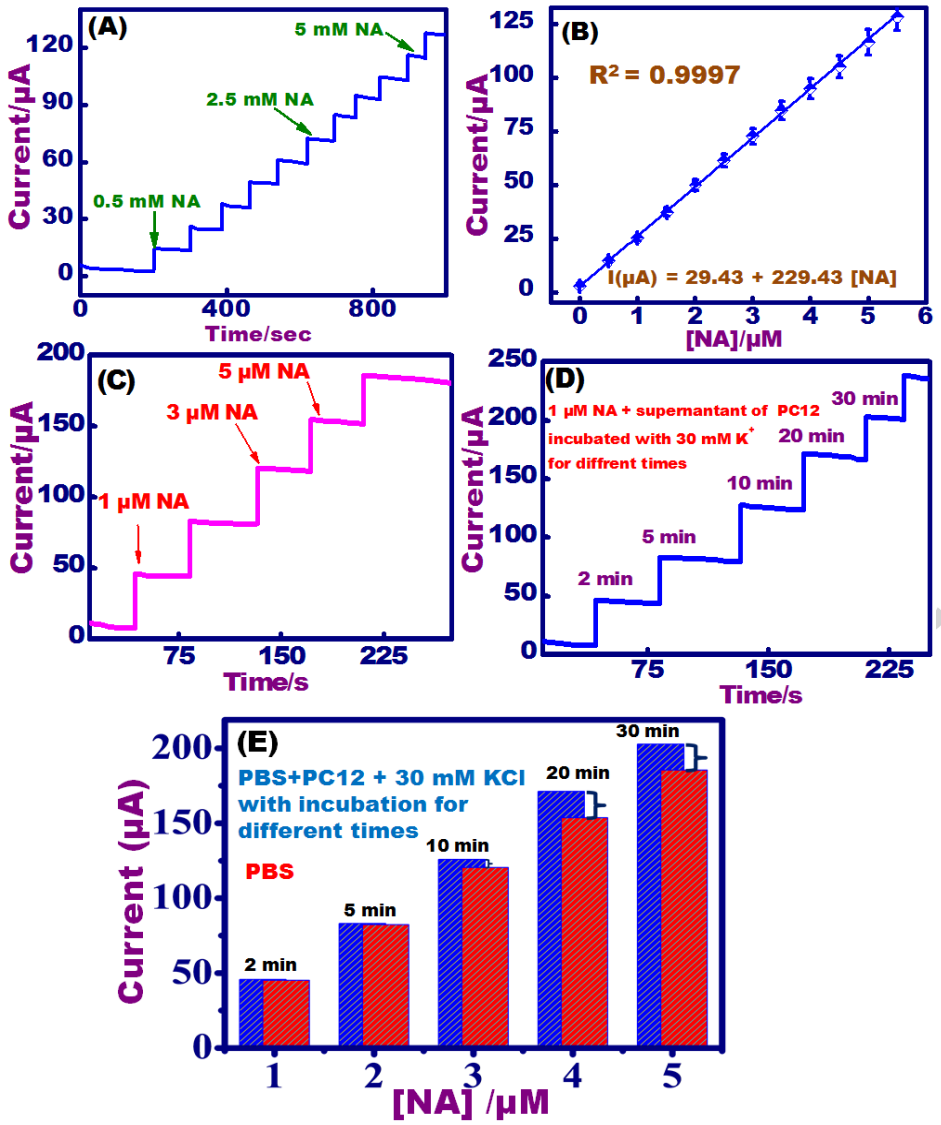

Figure 4. (A) The amperometric response of NA with successive addition from 0.5-5 µM on CNNB-1 nanoelectrode, and (B) The linear plot of concentration (µM) Vs the current (µA). (C &D) The amperometric response of NA addition in 0.1 M PBS pH=7 without and with PC12 induced by 30 mM KCl, (E) the column plot of concentration of noradrenaline with (blue column) and without (red column) PC12 (30 mM KCl) Vs the current (µA) at applied potential 0.17 V.

3.7. Monitoring of NA released from living cells (PC12) on CNNB-1 biosensor electrode

For the evaluation of neurological disorder (i.e., schizophrenia) based on disruption level of neurotransmitter, we selected healthy PC12 cells, which are like human neuronal cells. We assessed the suitability of the designed CNNB-1 biosensor electrode for control monitoring of an

in vitro NA released from PC12 cells (cells with extracellular noradrenaline). Many time-dependent methods using sophisticated techniques that do not have real-time responses have been used to monitor the NA release from cells, which usually require hours of work for sample collection and NA recognition using HPLC purification and mass identification (Lapainis et al. 2007; Nasirizadeh and Zare 2009; Wachman et al. 2004; Zhang et al. 2003). In comparison, Figures 4C-4E illustrate the real-time recording using CNNB-1 biosensor electrode, where NA released from PC12 was monitored with a current change within few seconds by using amperometric measurements.

K^+ induced noradrenaline released from PC12 cells was monitored through amperometric response under an applied potential of 0.17 V in 0.1 M PBS pH 7 (Figs. 4C and 4D). First, we directly investigate the various concentrations of noradrenaline in 0.1 M PBS solution (pH 7.0) as shown in Fig. 4C, where the amperometric response increased with step adding 1 μM NA. Similarly, we observe an amperometric response for NA released from PC12 as a constant addition of spiked 1 μM of NA with a supernatant of PC12 incubated with 30 mM KCl for various times (2, 5, 10, 20, and 30 min) (Fig. 4D). Figure 4E (red column) shows the column plot of NA-concentrations versus the current for CNNB-1 biosensor electrode in PBS (pH 7) for spiking NA, and standard NA with released NA from PC12 incubated with K^+ for each specific time (Fig. 4E (blue column)). Fig. 4E shows that the current response of NA with induced NA from PC12 was higher than that of spiked NA only. Cell membrane depolarization was reported by K^+ extracellular simulation in which the cell membrane depolarized and induced an influx of Ca^{2+} and Na^+ through the opening of voltage-sensitive Na^+ and Ca^{2+} channels (Shinohara et al. 2013). Increasing the level of intracellular Ca^{2+} enhances the release of NA from large dense core vesicles of the cells. The cells were stimulated by K^+ to depolarize the cells, as recorded from Fig. 4D, and represented in Fig. 4E (blue column). The released NA from PC12 increased as the incubation time with 30 mM K^+ was increased.

For further confirmation, PC12 cells were visualized using laser scanning confocal microscopy measurements after confirming the active wavelength region (Fig. 5). An in vitro model was adapted to study the interaction of CNNB-1 (20 μg/mL) and PC12 cells (5×10^5 cells/mL). Results indicate the positive detection of the released extracellular NA due to signal enhancement after incubation with CNNB-1 (Fig. 5D). DAPI (0.1 μg/mL) were used for PC12 cells nuclear counterstaining which indicates the localization within the cell and incubated cells with 30 mM K^+ (Fig. 5A&C). Figures 5(B&D) shows the colocalization and matching between CNNB-1 and DAPI counter stain which reflects a high degree of matching positivity and after

incubation for 30 min with 30 mM K^+. In addition, the low toxicity and high biocompatibility observed by confocal microscope visualization of the cells incubated with CNNB-1 (20 µg/mL) and control, where no damage or shrinkage on the cells membrane and the micro unit of CNNB-1 was clearly obtained with cells imaging. These results confirmed that the CNNB-1 can be used as a real in-vitro model for extracellular NA detection.

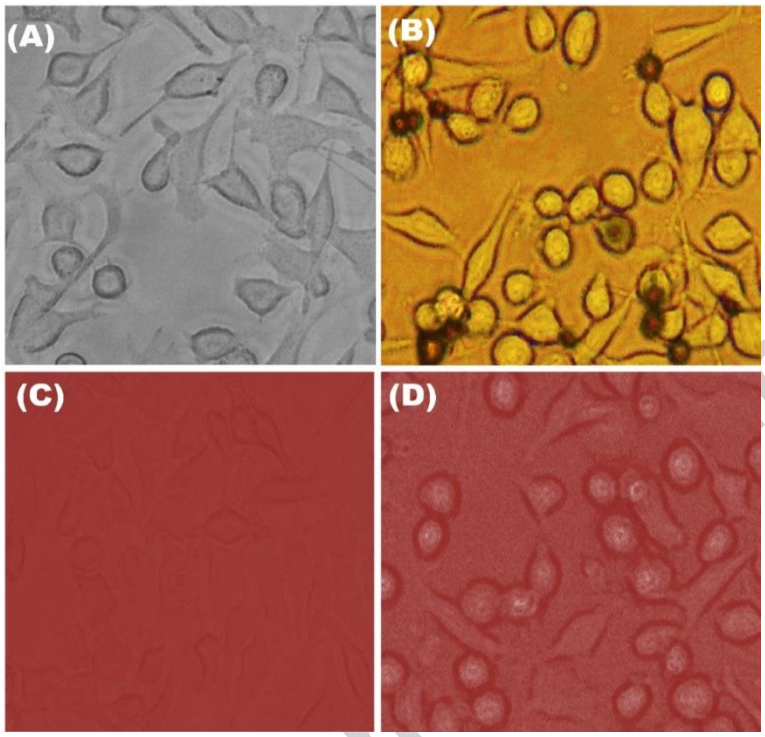

Figure 5. Confocal microscope images recorded at excitation wavelength of 488 nm and emission wavelength at 620 nm of control PC12 cells (A) and incubation of PC12 with 30 mM KCl for 30 min (C), PC12 cells with 20 µg/mL CNNB-1 for 30 min (B), and incubated PC12 +20 µg/mL CNNB-1with 30 mM KCl for 30 min (D).

4. Conclusion

The design of NA-biosensor electrode based on C-, N doped NiO broccoli-like hierarchy (CNNB) was successfully fabricated. Facile constructions of the CNNB biosensor electrodes with the controlled formation of single broccoli head (CNNB-1) or two asymmetric broccoli heads aligned by a trunk (CNNB-2) show the key elements in the sensitive and selective monitoring of NA. The jagged surface of CNNB head consists of nanotubes with an average size of 15 nm, and dominate meso-tunnel-like pore structure may lead to forming of multi-active sites, open-spaces, and easy mass transport at the electrode surface. The active doping of the NB broccoli-like hierarchy with CN nanospheres facilitate the electron transport and create abundant tubular vessels of active sites. The CNNB-1 biosensor exhibits high selectivity, sensitivity, stability, and reproducibility with low detection limit up to 6 nM for monitoring of NA. The

CNNB-1 biosensor shows low cytotoxicity and high biocompatibility as an in-vitro model for monitoring of NA released from living cells (PC12) under K^+ stimulation. The unique morphology of the CNNB-1 for NA-selectivity among interfering molecules may open their practical in-vitro application for clinical diagnosis and neuronal investigation.

References

Abdeleahab, A.A., 2016. Electroanalysis 28(8), 1901-1906.

Akhgar, M.R., Beitollahi, H., Salari, M., Karimi-Maleh, H., Zamani, H., 2012. Analy. Meth. 4(1), 259-264.

Akhtar, N., El-Safty, S.A., Abdelsalam, M.E., Shenashen, M.A., Kawarada, H., 2016. Biosens. Bioelectron. 77, 656-665.

Akhtar, N., El-Safty, S.A., Khairy, M., El-Said, W.A., 2015a. Sens. Actuat. B. chem. 207, 158-166.

Akhtar, N., El-Safty, S.A., Abdelsalam, M.E., Kawarada, H., 2015b. Adv. healthcare mater. 4(14), 2110-2119.

Ali, G.A., Teo, E.Y.L., Aboelazm, E.A., Sadegh, H., Memar, A.O., Shahryari-Ghoshekandi, R., Chong, K.F., 2017. Mater. Chem. Phys. 197, 100-104.

Andén, N.-E., Carlsson, A., Hillarp, N.-Å., Magnusson, T., 1965. Life sci. 4(2), 129-132.

Beitollahi, H., Mohammadi, S., 2013. Mater. Sci. Eng. C 33(6), 3214-3219.

Bergquist, J., Silberring, J., 1998. Rap. comm. mas. spect. 12(11), 683-688.

Braestrup, C., Nielsen, M., Scheel-Krüger, J., 1974. J. Neurochem. 23(3), 569-578.

Chandra, P., Son, N.X., Noh, H.-B., Goyal, R.N., Shim, Y.-B., 2013. Biosens.Bioelectron. 39(1), 139-144.

Chen, L., Feng, M., Zhan, H., 2014. RSC Adv. 4(58), 30689-30696.

Devnani, H., Satsangee, S.P., Jain, R., 2016. Mater. Today: Proceedings 3(6), 1854-1863.

Dong, S., Zhang, P., Liu, H., Li, N., Huang, T., 2011. Biosens. Bioelectron. 26(10), 4082-4087.

El-Safty, S.A., 2008. J. coll. interf. sci.319(2), 477-488.

El-Safty, S.A., Khairy, M., Shenashen, M.A., Elshehy, E., Warkocki, W., Sakai, M., 2015a. Nano Res. 8(10), 3150-3163.

El-Safty, S.A., Kiyozumi, Y., Hanaoka, T., Mizukami, F., 2008. Appl. Catal.A. 337(2), 121-129.

El-Safty, S.A., Sakai, M., Selim, M.M., Hendi, A.A., 2015b. ACS appl. mater. interf. 7(24), 13217-13231.

El-Safty, S.A., Shenashen, M.A, 2013. Sens.Actuat. B.183, 58-70.

El-Safty, S.A., Shenashen, M.A., Akhtar, N., Selim, M.M., Morsy, W.M., Yamaguchi, H., Kawada, S., Alhamid, A.A., Ohashi, N., Ichinose, I., 2017. Chemistry–An Asian Journal. doi. 10.1002/asia.201700666.

El-Safty, S.A., Shenashen, M.A, Ismael, M., Khairy, M., 2012. Adv.Functional Mater. 22(14), 3013-3021.

Glowinski, J., Kopin, I.J., Axelrod, J., 1965. J. Neurochem. 12(1), 25-30.
Hassan, D., El-Safty, S.A., Khalil, K.A., Dewidar, M., Abu El-Maged, G., 2016. Int. J. Electrochem. Sci 11, 8374-8390.
Hassen, D., El-Safty, S.A., Tsuchiya, K., Chatterjee, A., Elmarakbi, A., Shenashen, M.A., Sakai, M., 2016a. Sci. Rep. 6, 24330.
Hassen, D., Shenashen, M.A, El-Safty, S.A., Selim, M.M, Isago, H., Elmarakbi, A., El-Safty, A., Yamaguchi, H., 2016b. J. Pow. Sourc. 330, 292-303.
Huang, Q., Zhang, H., Hu, S., Li, F., Weng, W., Chen, J., Wang, Q., He, Y., Zhang, W., Bao, X., 2014. Biosens. Bioelectron. 52, 277-280.
Khairy, M., El-Safty, S.A., 2013. RSC Adv .3(45), 23801-23809.
Khairy, M., El-Safty, S.A., 2014. Sens. Actuat. B. 193, 644-652.
Khairy, M., El-Safty, S.A., 2015. J. Energy Chem. 24(1), 31-38.
Khairy, M., El-Safty, S.A., Ismael, M., Kawarada, H., 2012. Appl. Cataly. B. 127, 1-10.
Knez, M., Kadri, A., Wege, C., Gösele, U., Jeske, H., Nielsch, K., 2006. Nano Lett. 6(6), 1172-1177.
Knigge, U., Willems, E., Kjær, A., Jørgensen, H., Warberg, J., 1999. Endocrinology 140(8), 3713-3719.
Lapainis, T., Scanlan, C., Rubakhin, S., Sweedler, J., 2007. Analyt. Bioanalyt. Chem. 387(1), 97-105.
Liu, M., Liu, R., Chen, W., 2013. Biosens. Bioelectron. 45, 206-212.
Ma, Y., Zhao, M., Cai, B., Wang, W., Ye, Z., Huang, J., 2014. Biosens. Bioelectron. 59, 384-388.
Nasirizadeh, N., Zare, H.R., 2009. Talanta 80(2), 656-663.
Nikolelis, D.P., Petropoulou, S.S.E., Theoharis, G., 2003. Electroanalysis 15(20), 1616-1624.
Nikolelis, D.P., Raftopoulou, G., Siontorou, C.G., 2005. Electroanalysis 17(20), 1870-1877.
Salimi, A., Sharifi, E., Noorbakhsh, A., Soltanian, S., 2007. Biosens. Bioelectron. 22(12), 3146-3153.
Shenashen, M.A., Hassen, D., El-Safty, S.A., Isago, H., Elmarakbi, A., Yamaguchi, H., 2017a. Chem. Eng. J. 313, 83-98.
Shenashen, M.A., Hassen, D., El-Safty, S.A., Selim, M.M., Akhtar, N., Chatterjee, A., Elmarakbi, A., 2016. Adv. Mater. Interf. 3(24).
Shenashen, M.A., Kawada, S., Selim, M.M., Morsy, W.M., Yamaguchi, H., Alhamid, A.A., Ohashi, N., Ichinose, I., El-Safty, S.A., 2017b. Nanoscale 9, 7947-7959.
Shinohara, H., Sakai, Y., Mir, T.A., 2013. Analyt. biochem. 441(2), 185-189.
Sun, C.-L., Lee, H.-H., Yang, J.-M., Wu, C.-C., 2011. Biosens.Bioelectron. 26(8), 3450-3455.
Taei, M., Jamshidi, M.S., 2017. Microchem. J. 130, 108-115.
Wachman, E.S., Poage, R.E., Stiles, J.R., Farkas, D.L., Meriney, S.D., 2004. J.Neurosc. 24(12), 2877-2885.
Xiang, L., Deng, X., Jin, Y., 2002. Scripta Materialia 47(4), 219-224.
Yang, S., Feng, X., Wang, X., Müllen, K., 2011. Angew. Chemie. Inter. Ed. 50(23), 5339-5343.
Zhang, L., Qv, S., Wang, Z., Cheng, J., 2003. J. Chromatog. B 792(2), 381-385.
Zhang, X., Yan, W., Zhang, J., Li, Y., Tang, W., Xu, Q., 2015. RSC Adv. 5(80), 65532-65539.

Highlights

- Detection of ultra-trace concentrations of monoamine neurotransmitter in living cells
- C-, N-doped NiO broccoli-like (CNNB) provided highly sensitive biosensor
- Our finding provides high sensitivity up to 6 nM for NA-biosensing.
- C/N-doping enhance the ultrasensitive detection of NA in living cells " PC12"
- Simple, sensitive and selective assays of noradrenaline (NA).